

Supplementary information

Polarisation-dependent Raman enhancement in hexagonal boron nitride membranes

Jakub Rogoża¹, Johannes Binder¹, Kirill V. Voronin², Iris Niehues^{3,4}, Katarzyna Ludwiczak¹, Aleksandra K. Dąbrowska¹, Mateusz Tokarczyk¹, Rafał Bożek¹, Alexey Y. Nikitin^{2,5}, Rainer Hillenbrand^{3,5}, Roman Stępniewski¹, Andrzej Wyszomółek¹

¹ University of Warsaw, Faculty of Physics, Pasteura 5, 02-093 Warsaw, Poland

² Donostia International Physics Center (DIPC), Paseo Manuel de Lardizabal, 4, Donostia–San Sebastián 20018, Spain

³ CIC nanoGUNE BRTA and Department of Electricity and Electronics, UPV/EHU, Tolosa Hiribidea, 76, Donostia–San Sebastián 20018, Spain

⁴ University of Münster, Institute of Physics, Wilhelm-Klemm-Str. 10, 48149 Münster, Germany

⁵ IKERBASQUE, Basque Foundation for Science, Bilbao 48009, Spain

Additional Raman maps and AFM image of the grid structure

Figure S1 presents the Raman shifts and FWHM of the Raman E_{2g} fitted with a single Lorentzian peak function. It can be seen that there are slight changes in the Raman shift of the E_{2g} band of h-BN on the suspended part. No clear trend is observed for the FWHM of this peak. By comparing this with Figure 2(c), we can conclude that the changes in Raman shift do not correlate with the observed Raman enhancement effect. There are areas, such as the left side of the cross, that show almost no change in Raman shift but exhibit a clear enhancement of the signal.

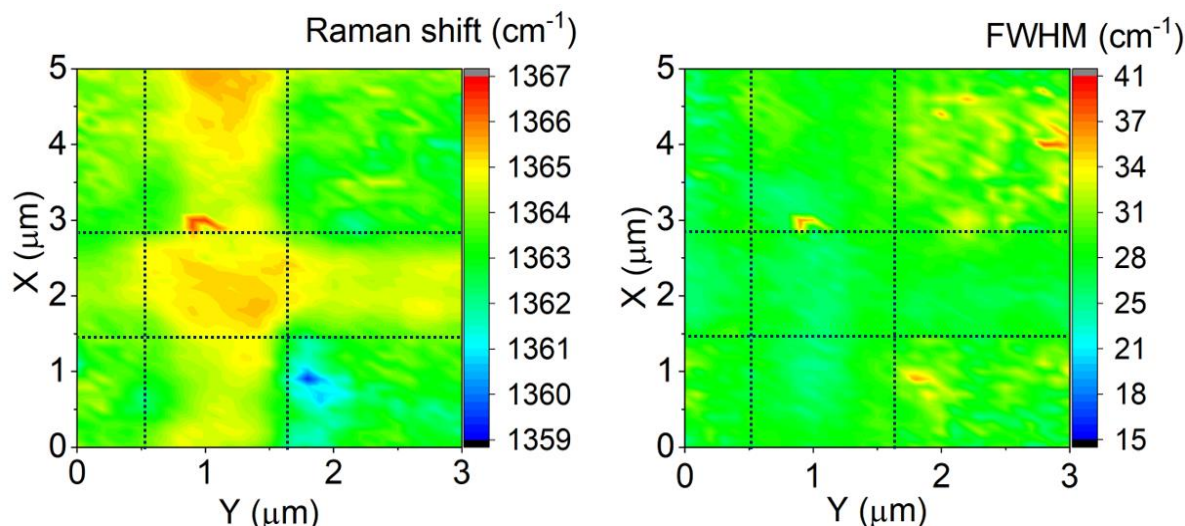


Fig. S1: False-colour maps of Raman shift and FWHM extracted from a Lorentzian peak fit to the spectra. The results correspond to the measurements shown in Fig. 2 c) in the main text. The dashed lines mark the position of the trenches.

These Raman measurement results are in good agreement with atomic force microscope (AFM) measurements shown in Figure S2.

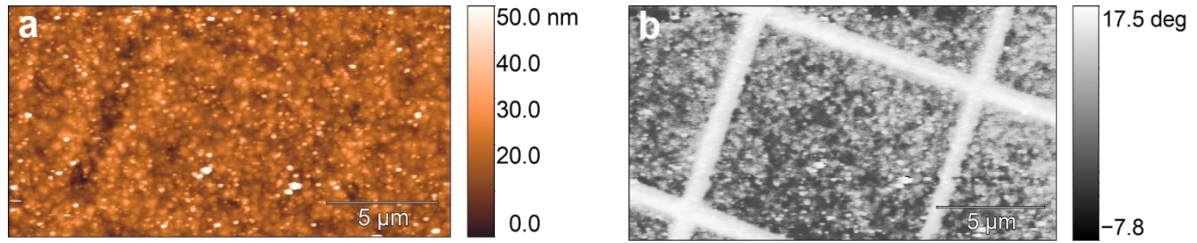


Fig S2: Atomic force microscopy results of the grid membrane structure presented in the main text. (a) Topography and (b) phase contrast image.

For these measurements, the membranes are clearly apparent in the phase contrast image but are not visible in the sample's topography. In some regions (e.g., the left side), some of the suspended areas show a slightly different height. However, we observe the enhancement effect across all regions of the sample, which rules out strain as the origin of the observed effects.

Additional Raman spectrum for the h-BN / graphene heterostructure

As indicated in Fig. 3 in the main text, the peak around 1360 cm^{-1} is a combination of the E_{2g} peak from h-BN and the D peak from graphene. To disentangle the two peaks, we conducted measurements with an excitation laser wavelength of 633 nm. The spectrum is shown in Fig. S3 and shows a clear separation of the two contributions.

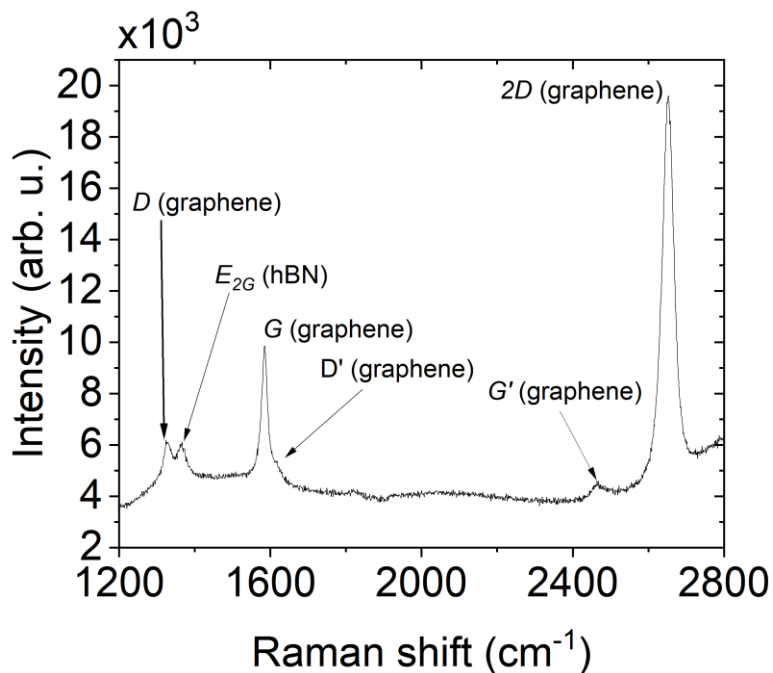


Fig. S3: Spectra of the graphene/h-BN/Ge structure measured with a 633 nm excitation laser. This spectrum showcases the presence of the D peak of graphene and the E_{2g} band of h-BN.

The presence of a D peak in the Raman spectrum is indicative of defects in the graphene layer. In our study, we required large graphene areas and consequently utilized graphene grown on copper, which was later transferred by chemically dissolving the copper substrate. Given the nature of graphene on copper and the significant luminescence background caused by copper oxides, it is difficult to evaluate the quality of the graphene on copper before its transfer. Nonetheless, previous studies have shown that photocorrosion etching of germanium beneath hBN/graphene does not damage the graphene layer (or other 2D materials), even when it is unsupported by h-BN [1]. Therefore, the defects observed in the Raman spectrum of graphene in our experiments are likely attributable to either the intrinsic quality of the graphene or the effects of the transfer process from copper to the germanium substrate, rather than being a direct result of the underetching process.

Different trench geometry

Figure S4 presents the electromagnetic full-wave simulations for a trench with slightly different geometry as the trench simulated in Figure 5 in the main text. Here, we assume an infinite in y-direction, 893 nm-deep, and 677 nm-wide trench in the germanium substrate, covered by a 30 nm-thick h-BN layer. The structure is illuminated from the top (air region) by a normally-incident plane wave polarized either along y or in x direction (parallel and perpendicular to the trench edge, respectively). We rounded off the edges with a curvature radius of 461 nm.

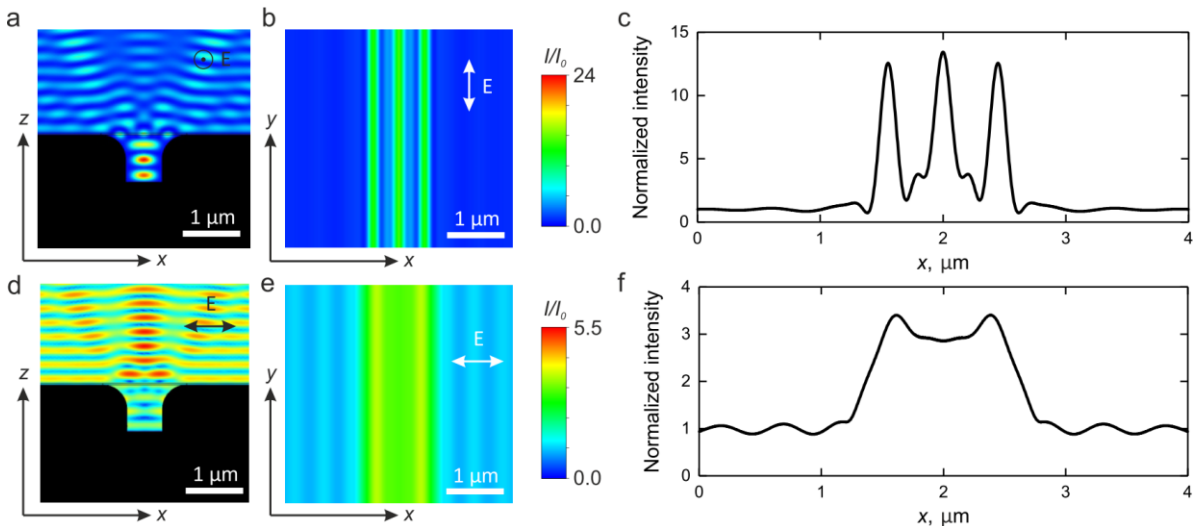


Fig. S4: Results of electromagnetic full-wave simulations. All panels represent the normalized electric field intensity, $(I/I_0=|E|^2/|E_0|^2)$, where I_0 is the intensity on the supported h-BN) for incident light at the wavelength of the laser (532 nm). a,d) the distribution of I/I_0 as a function of z,x for the polarisation of the incident light parallel and perpendicular to the membrane edge, respectively. The black colour represents the germanium substrate; the h-BN layer on top of the trench is shown by two black horizontal lines. b,e) the distribution of I/I_0 in the middle of the h-BN layer as a function of x,y , for parallel and perpendicular polarizations, respectively. c,f) display a cross-section of the distribution in b,e. Note that I/I_0 for incident light polarised perpendicular to the trench edge, is significantly weaker compared to the parallel polarisation case (compare the color scales).

Figure S4a clearly shows that for this geometry the third maximum (situated in the middle of the trench) is situated also inside the h-BN layer. The top view (x - y plane) presented in Fig. S4b, also clearly shows three lines. The cross-section shown in Fig. S4c, for which the intensities

were averaged over the whole h-BN thickness, shows that now the peak in the middle of the trench is even slightly more intense as the maxima situated close to the edges of the trench. This observation clearly indicates that the third maximum strongly depends on the actual depth of the trench, while the appearance of the maxima near the edges is a more robust effect. The situation of the third maximum can be regarded as similar to that of Interference Enhanced Raman Spectroscopy (IERS), where resonant conditions must be met to observe significant enhancement. The reliable observation of maxima near the edges, even for a single edge, as shown in Fig. 4 in the main text and Fig. S7, reduces the technical requirements regarding trench depth, which is important for potential implementation in real applications. For the case of the perpendicular polarization (Fig. S4d-f) the maximum in the middle vanishes and the maxima at the rounded edges are only slightly more intense than the average signal on the suspended h-BN.

Influence of the edge shape on the Raman signal enhancement

The distribution of the electromagnetic field for a wave polarized parallel to the trench edge, incident on two edges of different shape (sharp and fillet), is depicted in Fig. S5a and c. Fig. S5b illustrates the variation in light intensity for the two geometries under consideration. For the sharp edges the overall enhancement decreases for the parallel polarization (Fig. S5 b)). Fig. S5 d- f present analogous representations for light polarized perpendicular to the trench. In this case the two maxima vanish and a broad maximum appears in the middle of the trench. These figures underscore the significance of the trench geometry, formed during the etching process, on the observed enhancement effects.

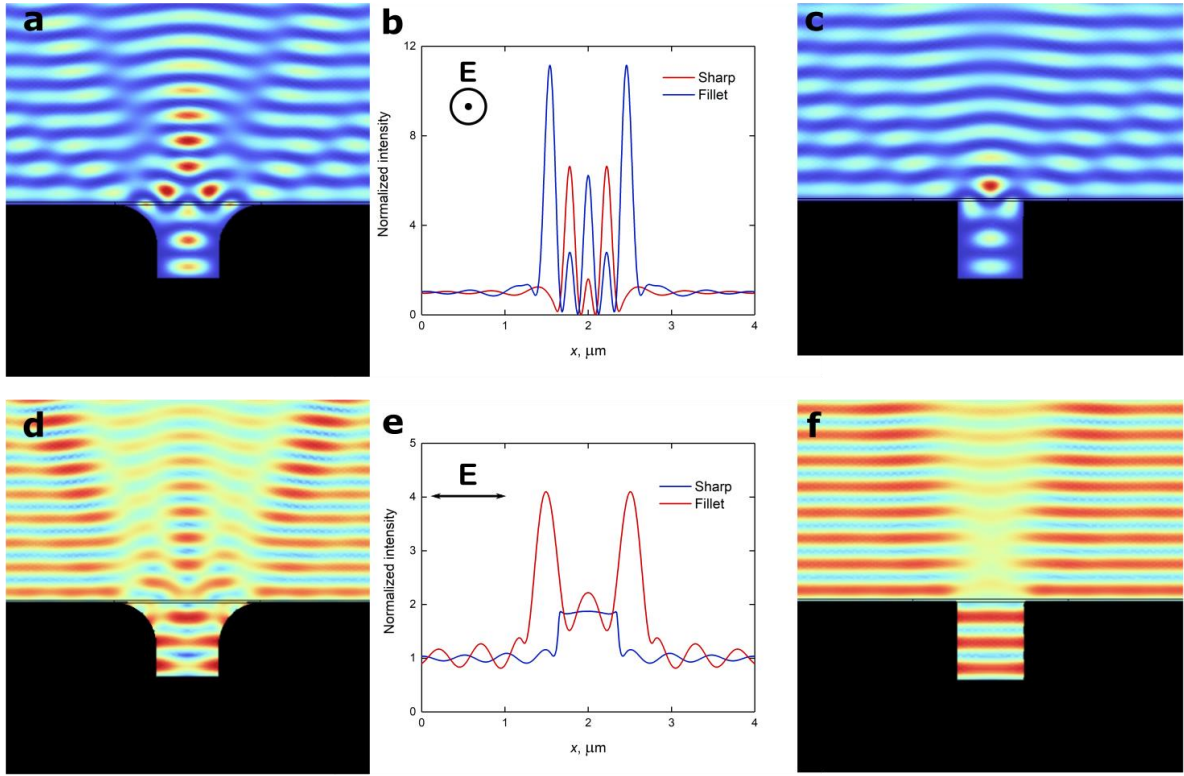


Fig. S5 a) and c) display the electromagnetic field distribution I/I_0 for waves polarized parallel to trench edges, for sharp and fillet edges. Figure b) depicts the field intensity variation, across the membrane for both geometries. Figures d), e), and f) present analogous simulations for light polarized perpendicular to the trench.

Estimation of the Raman enhancement factor from the simulated intensity enhancement factors

In order to estimate the Raman enhancement factor based on the simulated normalized electric field intensities, we calculated the dependency of the normalized maximum intensity (F) of the electric field as a function of the wavelength. Figure S6 show this relation for both polarizations, parallel and perpendicular to the trench edge. To obtain an estimation of the Raman enhancement factor, one has to multiply the intensity enhancement factor at the wavelength of the laser excitation $F_{\text{laser}} = I/I_0 = |E|^2/|E_0|^2$, where I_0 is the intensity on the supported h-BN, with the intensity enhancement factor at the wavelength of the Raman scattering signal F_{Raman} .

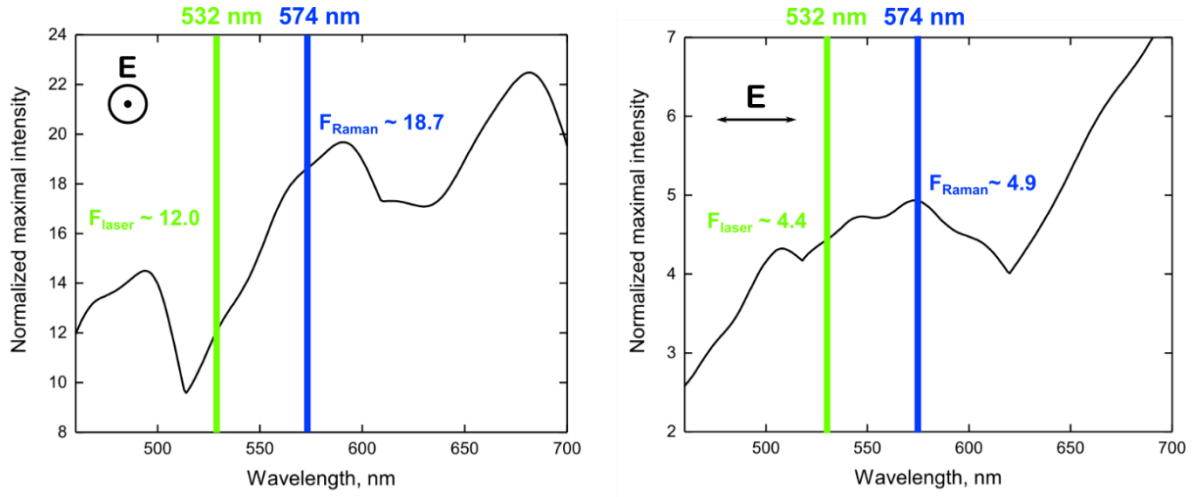


Fig. S6 shows the normalized maximum electric field intensity ($F=I/I_0=|E|^2/|E_0|^2$) as a function of wavelength for waves polarized parallel (a) or perpendicular (b) to the trench edges. The green rectangle indicates the laser wavelength (532nm) and the blue rectangle marks that position of the Raman h-BN E_{2g} band (574 nm) for this laser excitation. The green and blue numbers next to the rectangles show the value of the intensity enhancement factor F at the given wavelength.

Form Fig. S6 we can calculate:

$$\text{Raman enhancement factor (parallel polarization)} = F_{\text{laser}} \cdot F_{\text{Raman}} = 12.0 \cdot 18.7 = \mathbf{224.4}$$

$$\text{Raman enhancement factor (perpendicular polarization)} = F_{\text{laser}} \cdot F_{\text{Raman}} = 4.4 \cdot 4.9 = \mathbf{21.6}$$

These estimated values can be taken as an upper limit for experimentally observable Raman signal enhancements (at around 1367 cm^{-1}) for the geometry of the trench discussed in the main text.

Electromagnetic full-wave simulations for a single rounded edge

Figure S7 presents additional simulations for a single rounded edge. This case can be seen as the limiting case for two edges being very far from each other, as for the octagon-shaped structure described in the main text.

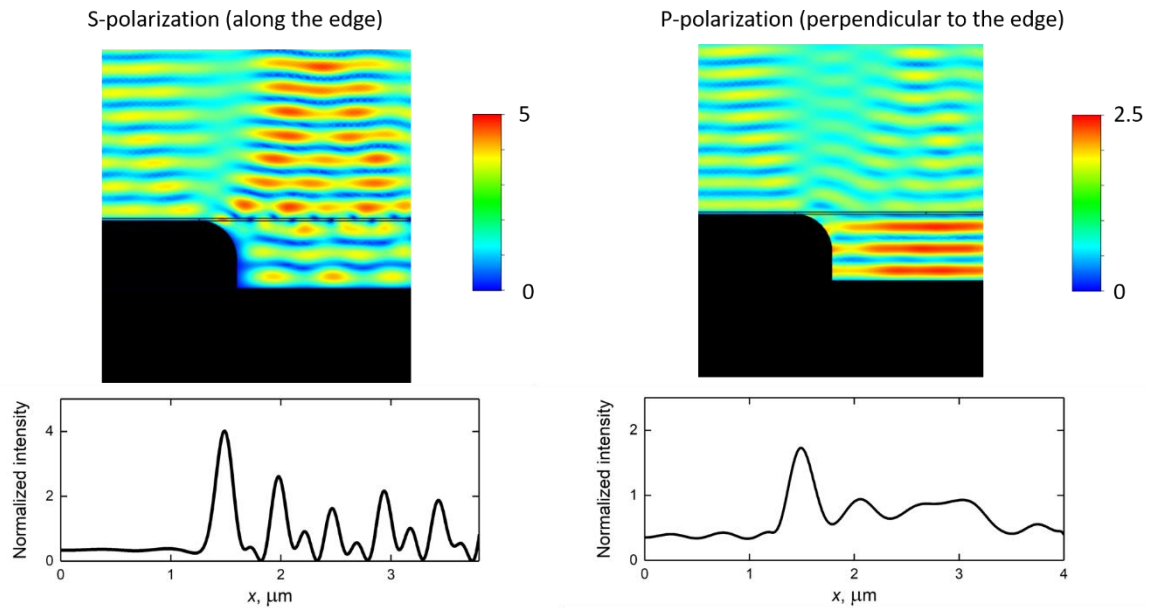


Fig S7: Additional simulation for the case of a single edge, corresponding to the octagon shaped membrane shown in the text. The simulations were performed using the excitation laser wavelength of 532 nm.

Despite significant changes in the electric field distribution, the normalized intensity for parallel polarization remains about twice as high compared to other polarizations. This indicates that the effect described in the main text is still observable, even for a single edge.

Electromagnetic full-wave simulations for a trench without h-BN layer

To further study the role of h-BN in the electric field distribution, we present electromagnetic full-wave simulations for the same trench geometry shown in the main text, but without h-BN layer.

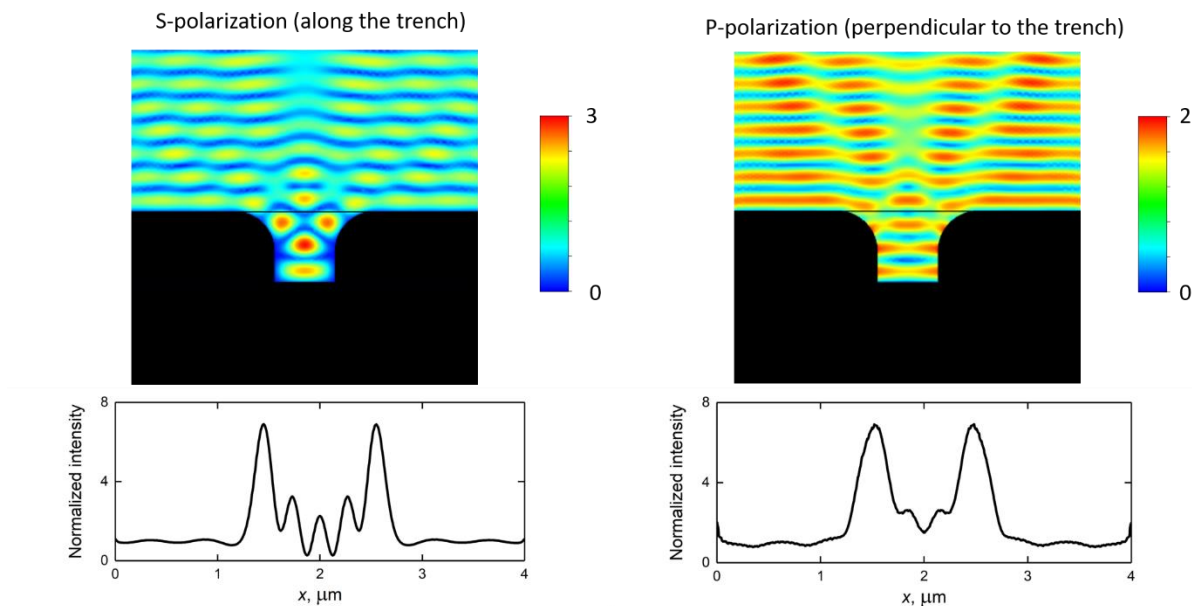


Fig S8: Additional simulations for the trench described in the main text, but without an hBN layer. The simulations were performed using the excitation laser wavelength of 532 nm.

A comparison between simulations with the h-BN layer (Fig. 5, main text) and simulations without the h-BN layer shows that the thin h-BN layer has a significant impact on the results. The maximum normalized intensity for polarization along the edge is much lower for the trench without the hBN layer. Additionally, the difference in maximum intensities for both polarizations is very small in the case without the h-BN layer. To further illustrate the influence of the hBN layer at other wavelengths, we present the normalized maximal intensities for different wavelengths for both polarizations in Figure S9.

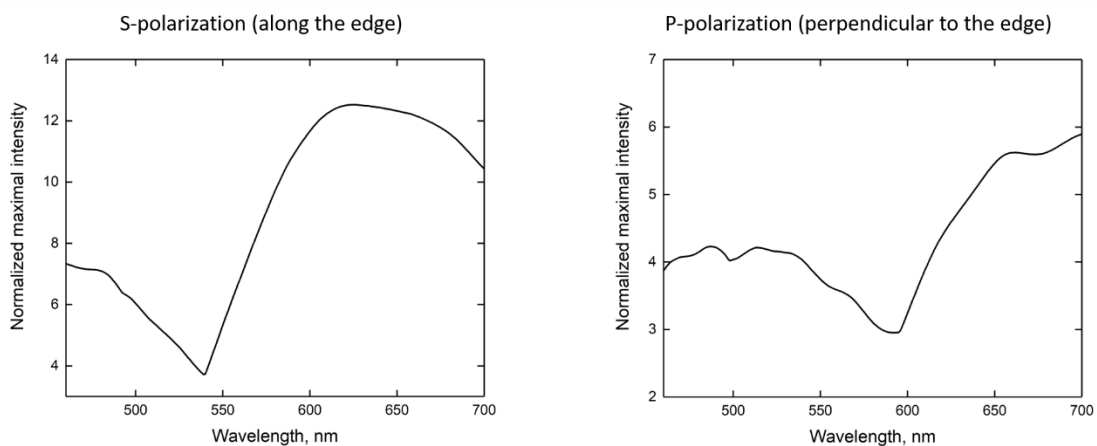


Fig S9: Wavelength dependence of the normalized maximum intensity for the case of a trench without an hBN layer.

The results show that the differences between the polarizations appear for longer wavelengths. The presented simulations show that the h-BN layer is directly influencing the final result. At the same time

it is difficult to present a simple rule of thumb, so in order to assess the result, simulations need to be performed.

Quality of h-BN layers before and after transfer

For the presented results, homogeneity on the sub-micrometer scale and the transparency of the layers in the visible region are very important. To the naked eye, the layer appears transparent after growth. To provide a more quantitative assessment, we present a UV-VIS absorption measurement of a 30 nm thick layer of h-BN in Figure S10.

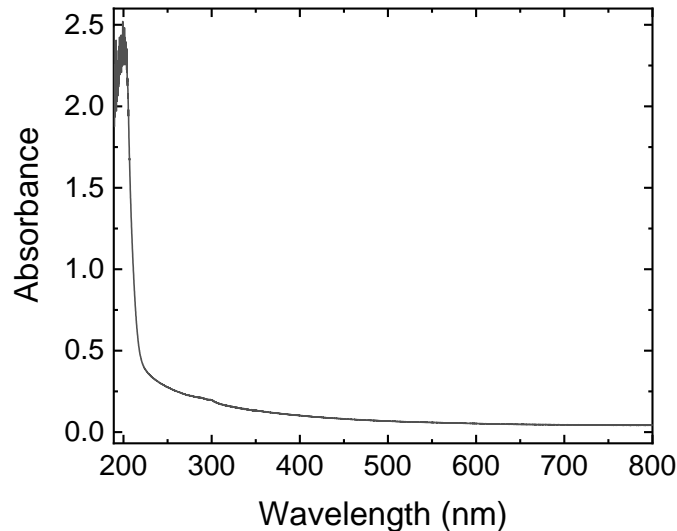


Fig S10: Absorbance spectrum of a 30 nm thick h-BN layer measured directly on a sapphire substrate. The response of a reference sapphire substrate was measured separately and was subtracted to extract the absorbance of the h-BN layer.

These absorption measurements of the h-BN on the sapphire substrate after growth do not show significant absorption in the visible range. The intense absorption at around 200 nm is caused by the direct excitonic resonances in h-BN.

To further show that the delamination process does not deteriorate the hBN quality we present a Raman map for the h-BN layer on sapphire, prior to the transfer.

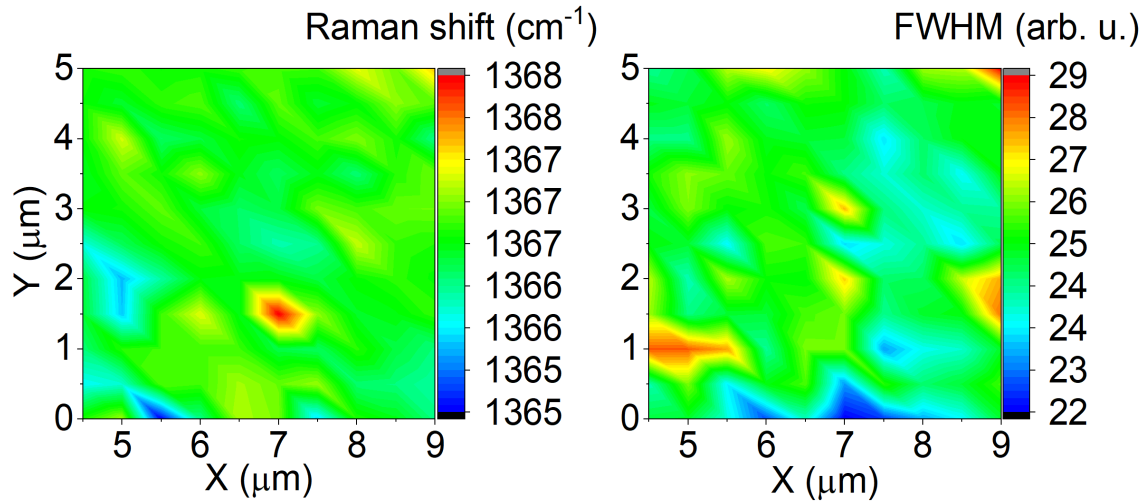


Fig. S11: Raman map of an as-grown h-BN layer on sapphire, prior to the transfer and etching process.

A comparison between the grid structure shown in Figure S1 and the pristine layer reveals that the overall Raman peak value slightly shifts due to the relaxation of the transferred layer. Additionally, the peak width distribution is narrower for the pristine h-BN, which can be attributed to differences between strained and unstrained regions, as discussed in Figures S1 and S2. However, the peak FWHM is very similar in both cases (see Fig. S1 and Fig. S11), indicating that the layer quality is comparable.

Additional example: tooth-shaped, octagonal membrane

Figure S12 presents an additional example of a tooth-shaped, octagonal etched membrane, measured with both parallel and perpendicular incident laser polarizations.

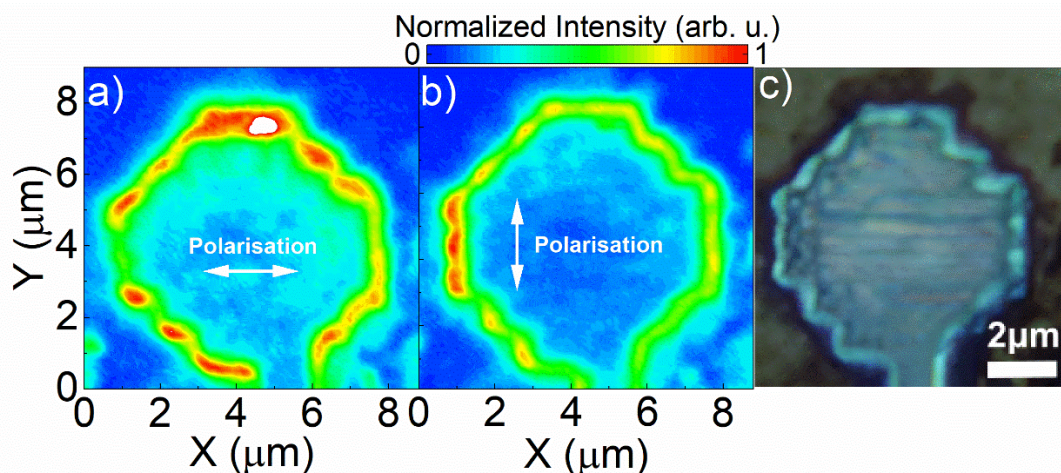


Fig. S12: False-color map of the E_{2g} Raman intensity with a laser polarisation set a) parallel to the X axis, b) parallel to the Y axis. c) Optical microscope image of a tooth-shaped, octagonal structure. The trench visible at the bottom was necessary to supply water beneath the h-BN surface during membrane etching.

The structure shown in Fig. S12 complements the results for the octagon-shaped structure presented in the main text (Fig. 4), as measurements with both parallel and perpendicular laser polarizations are provided. As expected, for incident polarization parallel to the X-axis,

the sidewalls that align with the laser polarization show an enhanced Raman signal. In addition to the long parallel sidewall, an enhancement is also observed on the corresponding sidewalls of the tooth-shaped structures. Similarly, laser excitation with polarization parallel to the Y-axis enhances the Raman signals in different regions, particularly along the left sidewall and the parallel sidewalls of the tooth-shaped structure, as seen most clearly in the lower right edge of the membrane.

Despite the overall very good agreement with expectations, some deviations are observed. The most notable example is a white area on the top sidewall, which exhibits a very strong enhancement (beyond the scale used). A close look at the optical image in Fig. S12c reveals that this feature correlates with a dark spot in the optical image. This observation suggests that the sidewalls must be well-defined to achieve a homogeneous Raman enhancement, as any deviation may lead to unexpected results.

Bibliography:

[1] - Binder, J.; Rogoza, J.; Tkachenko, L.; Pasternak, I.; Sitek, J.; Strupinski, W.; Zdrojek, M.; Baranowski, J. M.; Stepniewski, R.; Wyszomolek, A. Suspended Graphene on Germanium: Selective Local Etching via Laser-Induced Photocorrosion of Germanium. *2D Materials* 2021, 8, 35043.